**This document was prepared in conjunction with work accomplished under Contract No. DE-AC09-96SR18500 with the U. S. Department of Energy.**

## DISCLAIMER

# STRESS CORROSION CRACKING OF CARBON STEEL WELDMENTS

**Poh-Sang Lam**
Savannah River National Laboratory
Aiken, SC 29808, USA

**Changmin Cheng**
University of South Carolina
Columbia, SC 29208, USA

**Yuh J. Chao**
University of South Carolina
Columbia, SC 29208, USA

**Robert L. Sindelar**
Savannah River National Laboratory
Aiken, SC 29808, USA

**Tina M. Stefek**
Savannah River National Laboratory
Aiken, SC 29808, USA

**James B. Elder, III**
Savannah River National Laboratory
Aiken, SC 29808, USA

## ABSTRACT

An experiment was conducted to investigate the role of weld residual stress on stress corrosion cracking in welded carbon steel plates prototypic to those used for nuclear waste storage tanks. Carbon steel specimen plates were butt-joined with Gas Metal Arc Welding technique. Initial cracks (seed cracks) were machined across the weld and in the heat affected zone. These specimen plates were then submerged in a simulated high level radioactive waste chemistry environment. Stress corrosion cracking occurred in the as-welded plate but not in the stress-relieved duplicate. A detailed finite element analysis to simulate exactly the welding process was carried out, and the resulting temperature history was used to calculate the residual stress distribution in the plate for characterizing the observed stress corrosion cracking. It was shown that the cracking can be predicted for the through-thickness cracks perpendicular to the weld by comparing the experimental $K_{ISCC}$ to the calculated stress intensity factors due to the welding residual stress. The predicted crack lengths agree reasonably well with the test data. The final crack lengths appear to be dependent on the details of welding and the sequence of machining the seed cracks, consistent with the prediction.

**Keywords:** GMAW, SCC, IGSCC, finite element analysis, welding simulation, residual stress, stress intensity factor, $K_{ISCC}$.

## INTRODUCTION

A285 carbon steel has been used to construct high level nuclear waste storage tanks. The steel plates were joined by Gas Metal Arc Welding (GMAW). It was found that the weldments are susceptible to intergranular stress corrosion cracking (IGSCC) in a region spanning the weld. The cause of cracking is attributed to nitrate stress corrosion cracking driven by the residual stress due to the welding of the large plates during construction. The stress corrosion cracking (SCC) has occurred in or near the welds of some storage tanks containing a corrosive chemistry, and that were non-stress relieved. This degradation phenomenon has been investigated by experimentation to provide information on crack formation in welded plates, prototypic to tank construction.

The SCC experiment used two 30.5 cm x 30.5 cm (1 ft. x 1 ft.) welded plates following the carbon steel tank fabrication procedure used in 1950's. The corners of the plates were constrained during welding to simulate the large plate welding in the tank construction. Seed cracks were fabricated across and parallel to the weld using electric discharge machining (EDM). One of the plates was stress relieved and the other was as-welded. These test specimens were submerged in 5 molar (5M) sodium nitrate ($NaNO_3$) solution at about 90 °C up to 10 weeks. Periodic inspections were performed. It is found that the as-welded plate exhibited cracking within two weeks of exposure, and the stress-relieved plate remained intact. This test has successfully demonstrated that the SCC can indeed occur in non-stress relieved A285 tanks, and the stress relief procedure that was implemented for later tank construction effectively removed the susceptibility of this material degradation mechanism.

A three-dimensional thermo-mechanical finite element analysis [1] was performed to determine the welding residual stress by using the temperature history calculated from a heat transfer analysis to simulate the process of GMAW [2-4]. Traction-free cracks were then introduced to the finite element model and the re-distributed residual stress was used to calculate the crack tip stress intensity factors (K) along the crack front of a seed crack. Coupled with previous published experimental data for $K_{ISCC}$ (the threshold stress intensity factor below which no SCC can occur) [5], the theoretical IGSCC lengths can be predicted and are compared to the experimental measurement. In view of many uncertain variables during the welding process, the agreement between the test results and the numerical prediction is reasonably well. The analysis also indicated that the sequence of fabricating seed cracks may influence the final residual stress distribution and eventually, the final crack length.

## EXPERIMENT

ASTM A285 Grade B carbon steel was the primary material of construction of the 1950's high level radioactive waste storage tanks. The original vintage of the steel is not available. Based on the chemical composition attributes, A285 Grade C, vendor Heat R934 was chosen for the fabrication of the laboratory specimens in this study. The chemical composition in weight percent (wt.%) is: C – 0.075, Mn – 0.531, P – 0.008, S – 0.022, Si – 0.202, Cu – 0.259, Ni – 0.098, Cr – 0.083, Mo – 0.021, Sn – 0.028, Al – 0.002, Nb – 0.001, V – 0.000. The mechanical properties from the vendor information are: tensile strength – 407 MPa (59 ksi), yield strength – 303 MPa (44 ksi), elongation – 28% for gage length 20.3 cm (8 in.).

Each of the two 30.5 cm x 30.5 cm (12 in. x 12 in.) test specimens was fabricated by joining two A285 carbon steel plates (Fig. 1) with the GMAW procedure that was used in 1950's for constructing the high level radioactive waste storage tanks. The thickness of the plate is 15.88 mm (0.625 in.) and is identical to that of a typical storage tank. To simulate the actual welding of large plates in the storage tanks, the corners of the plates were constrained during welding. One of the specimen plates was heat treated with the standard treatment for stress relief and the other remained as-welded. To fully utilize the test plates, nine seed cracks were fabricated with EDM. Figure 2 shows the crack arrangement: V1, V2, and V3 are the vertical cracks across the weld through the thickness of the plate; V4 and V5 are the part-through vertical cracks; P1, P2, P3, and P4 are the part-through parallel cracks. The seed crack lengths were nominally 12.7 mm (0.5 in.) and the depth was 25% of the plate thickness for the part-through cracks.

Subsequently, these specimen plates were submerged in the solution of 5M $NaNO_3$ at about 90 °C. The solution was prepared with regent grade compound and distilled water, which is known to cause SCC and has been used as a surrogate solution for high level radioactive waste in developing chemistry controls in the tanks for corrosion prevention [6].

Periodic visual examinations were performed frequently, and non-destructive ultrasonic (UT) and magnetic particle (MT) tests were conducted at the end of testing. Without external loading, the experiment showed that cracking occurred in the as-welded plate as early as within two weeks of exposure to the solution, while the stress relieved plate did not show any evidence of cracking in 10 weeks. It can be concluded that the A285 carbon steel weldment is susceptible to SCC unless it is stress relieved.

Figure 3 is the magnetic particle test results of the as-welded plate after the test was complete. The through-thickness cracks (V1, V2 and V3) exhibit significant crack extension and the final crack lengths on both sides of the plate are labeled. The ultrasonic testing confirmed that the cracking only occurred in these vertical cracks, and the subsurface crack profiles through the thickness can be seen in Figure 4.

Note that the final crack lengths are significantly different for V1, V2, and V3 (ranging from 4 to 15 cm). The finite element analysis described later in this paper provides a partial explanation. Nevertheless, this experiment has clearly shown that: 1) SCC can occur due to the welding residual stress alone; and 2) the stress relief procedure has effectively removed the residual stress and susceptibility to SCC in the welded plates.

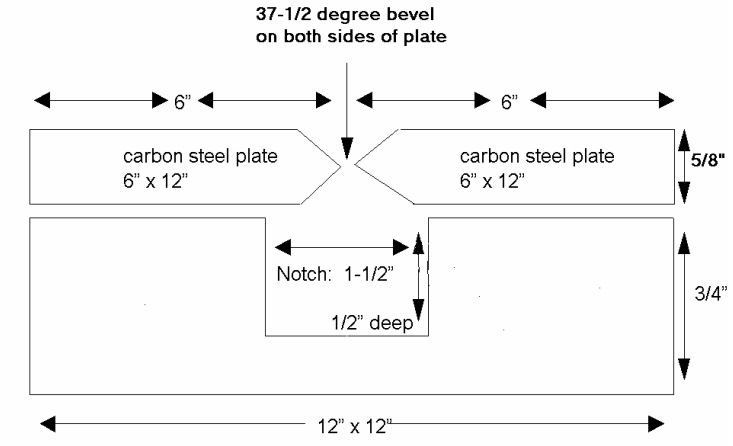


Figure 1 Welding of the A285 carbon steel plates.

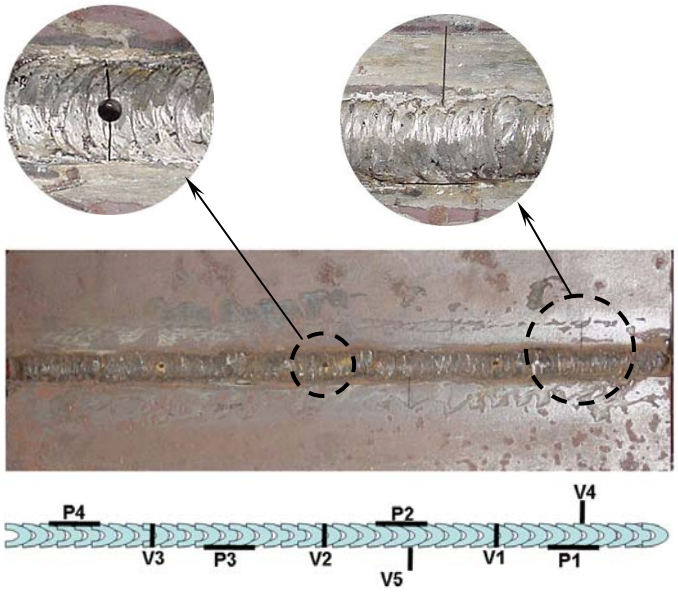


Figure 2 Welded sample and seed crack arrangement.

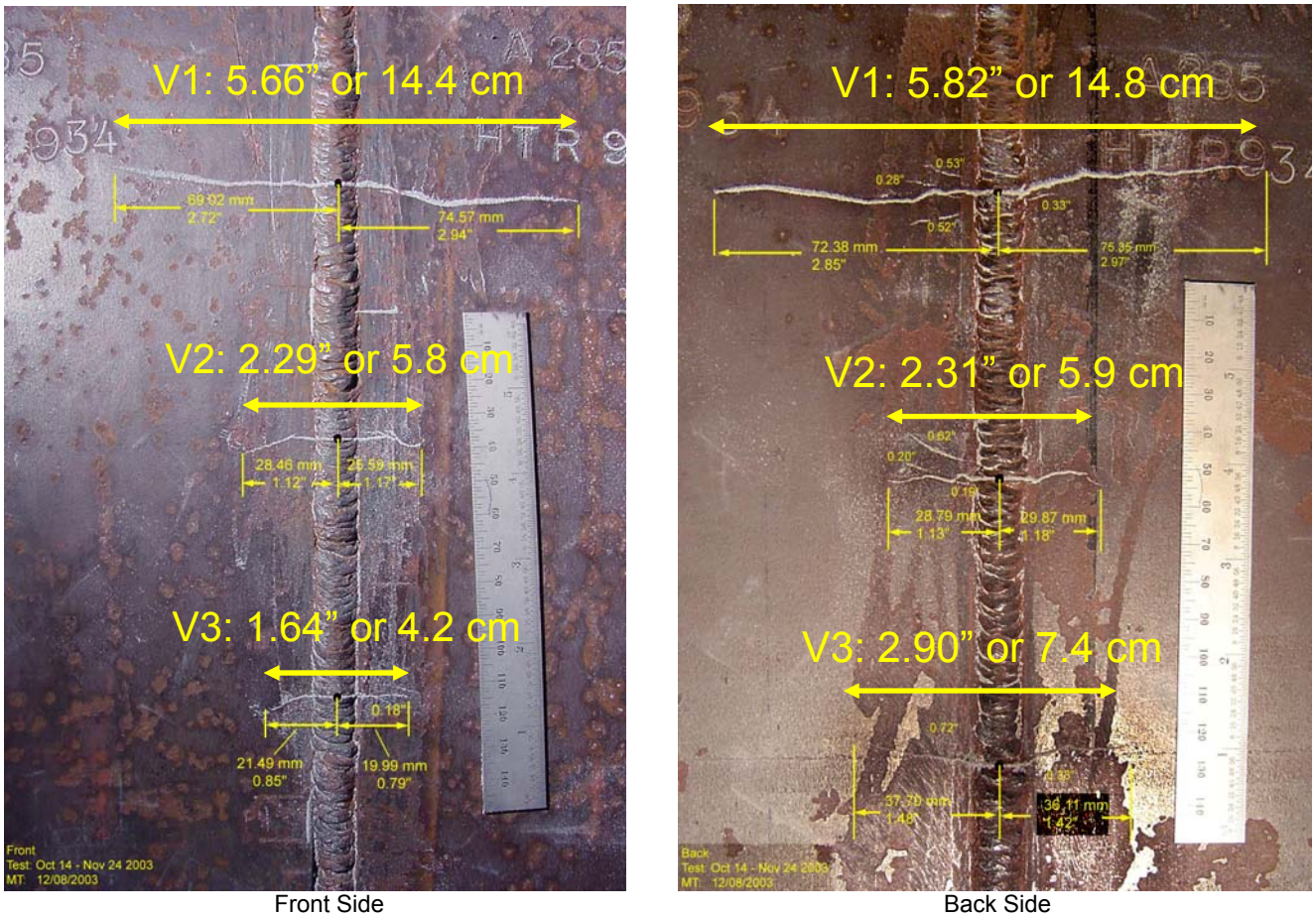


Front Side Back Side

Figure 3 Stress corrosion cracking of the as-welded plate (magnetic particle testing).

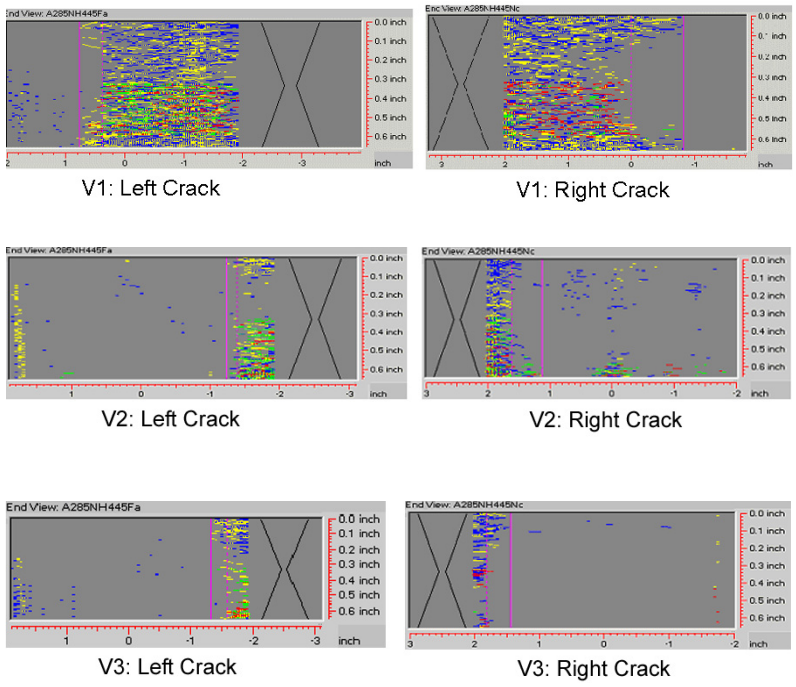


Figure 4 Ultrasonic testing shows the final subsurface profiles of the through-thickness cracks

.

## FINITE ELEMENT ANALYSIS

A three-dimensional finite element analysis was developed to benchmark the experimental results of the final SCC lengths [7]. The size of the specimen plate is 30.48 cm x 30.48 cm x 1.59 cm (length x width x thickness). Because of symmetry, only one-half of the plate is modeled (except in the analysis of the parallel crack P2 discussed later). The finite element model in Figure 5 contains 6780 eight-node brick elements with 8723 nodes. This mesh was used in both the heat transfer and the stress analyses.

The heat transfer analysis to simulate the GMAW was conducted with WelsSim, a three-dimensional welding finite element program developed by Chao et al. [2-4]. The detailed mesh in the V-groove area is shown in Figure 6, where the six passes are identified. The calculated temperature history from the entire welding simulation is input to the ABAQUS finite element program [1] for calculating the as-welded residual stress by a thermo-mechanical procedure. This residual stress field is re-distributed after the traction-free seed cracks are introduced into the finite element model. These cracks may be allowed to grow in a self-similar manner by creating newer traction-free surfaces. As a result, the stress intensity factor as a function of crack length can be established. Comparing with the $K_{ISCC}$ (35.2 MPa√m or 30 ksi√in) which was determined previously [5], the predicted SCC lengths can be obtained.

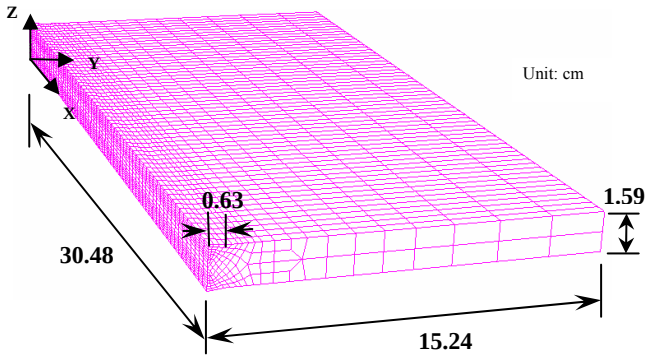


Figure 5 Three-dimensional finite element model for welding simulation and for the subsequent thermo-mechanical analysis.

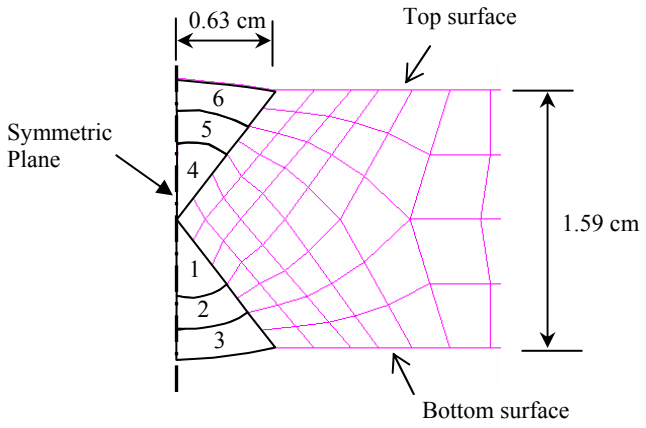


Figure 6 Detailed finite element mesh in the V-grooves showing the six passes of welding.

**Heat Transfer Analysis for Welding Simulation**

In the process of GMAW, the heat source provided by the weld arc melts the metal in the welding region. Therefore it is a process of heat absorption and heat diffusion inside the plate. The governing equation is:

$$\rho c_p\left(\frac{\partial T}{\partial t} - v\frac{\partial T}{\partial x}\right) = \nabla\cdot(k\nabla T) + \dot{q} \qquad (1)$$

where $\rho$ is the material density, $c_p$ is the specific heat, T is temperature, t is time, v is the welding speed, x is coordinate axis in the welding direction, k is the conductivity coefficient, and $\dot{q}$ represents heat input density.

An internal heat source is used in the thermal analysis. The heat input density is assumed to be constant in the thickness direction (Z direction in Figure 5). In the plane perpendicular to the thickness direction (XY plane in Figure 5), the heat source is assumed to have a Gaussian distribution. This type of heat source has been used by many researchers to approximate the actual distribution of heat source during welding. The equation for the heat input density, $\dot{q}$ (watt per unit volume), is:

$$\dot{q} = \dot{q}_{max}\exp\left(-cr^2\right) \qquad (2)$$

where $\dot{q}_{max}$ is the peak value at the center of the heat source, c is a constant, and r is the distance from the arc center. For a Gaussian distribution of the heat flux, 95% of which is confined within the area of a circle with radius $r_{arc}$. From [8],

$$c = \frac{3}{r_{arc}^2}$$

Integrating Eq. (2) over the volume gives the expression for the total heat input, q:

$$q = \int_{z=0}^{z=d}\int_{\theta=0}^{\theta=2\pi}\int_{r=0}^{r=\infty}\dot{q}_{max}\exp\left(-cr^2\right)\,rdrd\theta dz = \frac{\pi d\dot{q}_{max}}{c} \qquad (3)$$

where d is the thickness of the plate.

For GMAW process, $q = UI\eta$, where U, I, and $\eta$ are the welding voltage, current, and arc efficiency respectively. In the present work, the following welding parameters were used in fabricating the test specimens and in the analysis:

Current (I):90~105 A
Voltage (U): 18~21 V
Welding speed: 0.15 cm/s
Welding Efficiency: 67%
Weld pass: 6
Weld arc radius: 0.4 cm

Welding time per pass: 206 s

The average values of the current (I) and the voltage (U) were used in the calculation. They are, respectively, 97.5 A and 19.5 V. Therefore, the total heat input is q= 1274 watts per pass.

On the plate surfaces, the total heat loss ( $q_{loss}$ ) through the combination of thermal convection ( $q_{conv}$ ) and radiation ( $q_{rad}$ ) can be obtained from the equation [9]:

$$q_{loss} = q_{conv} + q_{rad} = h^* A(T - T_{sur}) \qquad (4)$$

where A is the surface area, T is current temperature, $T_{sur}$ is the ambient temperature, and $h^*$ is given by the following equation [9]:

$$h^* = \left| h + \varepsilon\sigma(T + T_{sur})(T^2 + T_{sur}^2) \right| \qquad (5)$$

where h is the thermal convection coefficient (15 W/m$^2$K in this study), $\varepsilon$ is the radiation emissivity, and $\sigma$ is the Stefan-Boltzmann constant (5.67 x 10$^{-8}$ W/m$^2$K$^4$). On the surface of the mild steel, $\varepsilon$ = 0.3 at T = 1000 K; and $T_{sur}$ is 20 $^o$C (293 K). By substituting these values into equation (6), $h^*$ is obtained as 39 W/m$^2$K.

**Thermal Properties**

In this analysis, the thermal properties for both base metal (A285 carbon steel) and for filler metal (E6010) are assumed to be identical, as collectively plotted in Figure 7. When the temperature reaches the melting point (1532 $^o$C), a weld pool is formed. To model the high thermal convection in the weld pool, the conductivity coefficient is set to five times higher than that at the melting temperature [10]. In addition, the latent heat of the metal is 247 kJ/kg.

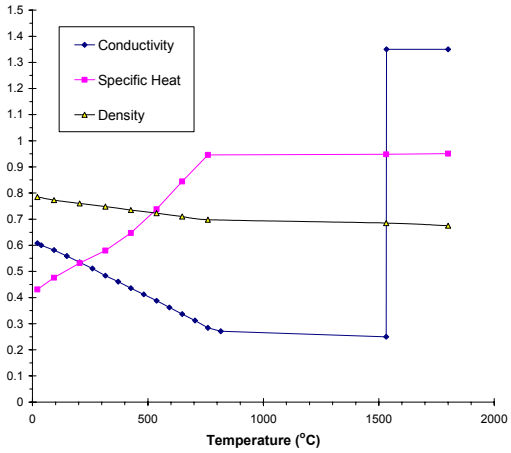


Fig 7 Temperature dependent thermal conductivity (J/cm•s•$^o$C), specific heat (J/g•$^o$C), and density (10g/cm$^3$) of the base and the filler metals.

The WeldSim program [2-4] uses dummy elements in the void space in the weld groove before the torch arrives to deposit the weld metal. The thermal material properties for the dummy elements, such as the density and the thermal conductivity, are set to 5% of the property values of the filler metal.

**Welding Residual Stress Analysis**

The temperature history calculated from the welding simulation with WeldSim [2-4] is input to the ABAQUS [1] for thermal stress analysis. For convenience, the finite element model used in WeldSim (Fig. 5) was adapted to ABAQUS. Again, the dummy elements are used before the welding torch arrives. This is achieved by applying the element-removing and element-reactivating features in ABAQUS. This technique has been studied and used in many models [11,12] to simulate the material deposit region in the weld groove. When the temperature history is applied to the thermo-mechanical analysis, the appropriate clamping conditions to constrain the plates are applied. The final equilibrium stress state is the welding residual stress.

**Mechanical Properties**

Following a previous work involving the welding of the same materials [13], the mechanical properties for both the base metal (A285 carbon steel) and the weld filler material (E6010) are assumed to be identical, except the yield stresses. In general, the yield stress of the filler material is higher than that of the base metal. Therefore, the yield stress of the filler metal is set to 1.48 times that of the base metal [13]. The Temperature dependent mechanical properties are plotted in Figures 8 to 10.

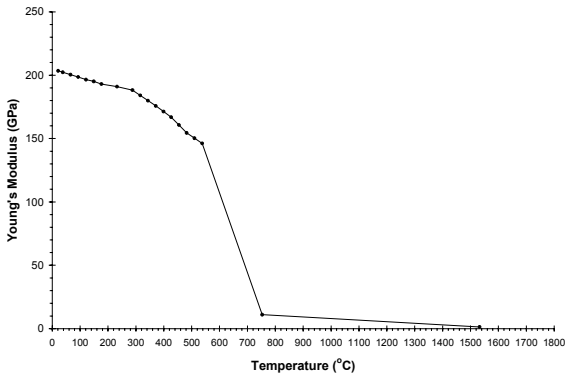


Figure 8 Temperature dependent Young's modulus

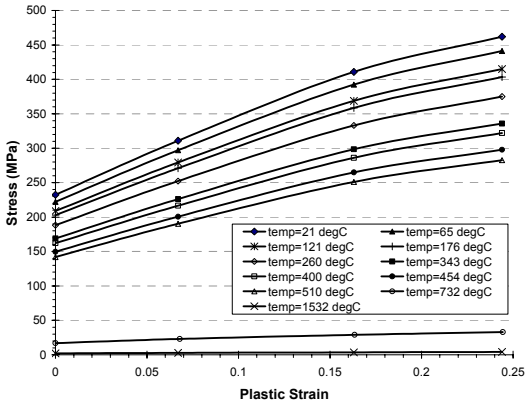


Figure 9 True stress-true plastic strain curves of the base metal (A285 carbon steel)

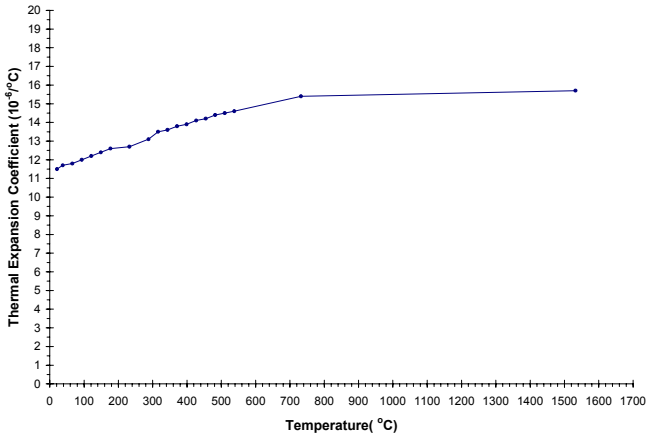


Figure 10 Temperature dependent thermal expansion coefficient (unit: $10^{-6}/^{o}C$)

**Analysis of Stress Corrosion Cracking**

Figure 2 shows the seed crack arrangement in the specimen plates for stress corrosion cracking test in an aggressive chemistry environment (5M $NaNO_3$ at 90 °C). Crack growth only occurred in the case of the through-thickness vertical cracks (V1, V2, and V3) across the weld. The interaction between the welding residual stress and the seed cracks is investigated in this section.

The finite element mesh in Figure 5 is refined especially in the seed crack locations for the subsequent fracture analysis. The initial stress for the refined mesh is established by mapping the previously calculated residual stress through the ABAQUS mesh-to-mesh solution mapping feature [1]. The cracks are then introduced to the finite element model by creating new, traction-free surfaces. The ABAQUS algorithm will equilibrate the unbalanced stresses in the new model due to the boundary change.

Through-thickness Vertical Cracks. The mesh near the crack locations is refined as seen in Figure 11. By mapping the solution in Figure 11a (shorter crack) to Figure 11b (longer crack) and then performing stress equilibrium calculations, the crack growth simulation can be approximated. The resulting redistributed stresses are used to calculate the stress intensity factors at the crack tip nodes along the crack front. The calculated stress intensity factors for V1, V2, and V3 along the straight crack fronts through the thickness of the plate are mostly greater than the threshold SCC stress intensity factor ($K_{ISCC}$= 35 MPa$\sqrt{m}$ ). This indicates that these cracks have a tendency to grow, as seen in Figure 3.

Part-Through Cracks. No SCC for the part-through seed cracks has occurred in the experimental program discussed earlier in this paper. Therefore, no advancing crack is modeled by the finite element method as was carried out for the through-thickness vertical cracks. The stress intensity factors due to the as-welded residual stress are calculated. In the present case, the parallel crack P2 is selected for analysis (Fig. 12). Because of the asymmetry due to the presence of P2, a full plate must be modeled. Therefore, the as-welded residual stress distribution obtained earlier with a symmetric mesh is mapped to both sides of the weld in a model containing P2. This original residual stress is redistributed after P2 is created in the model. Because the current finite element mesh consists of only brick elements, the semicircular crack front is closely approximated by the rectangular finite element boundary in the mesh. The stress intensity factors are calculated at these nodal point along the finite element crack front. It can be shown that the maximum stress intensity factor is 17 MPa$\sqrt{m}$, which is much below the $K_{ISCC}$ (35 MPa$\sqrt{m}$). This is consistent with the experimental observation that no crack growth has been detected for this seed crack.

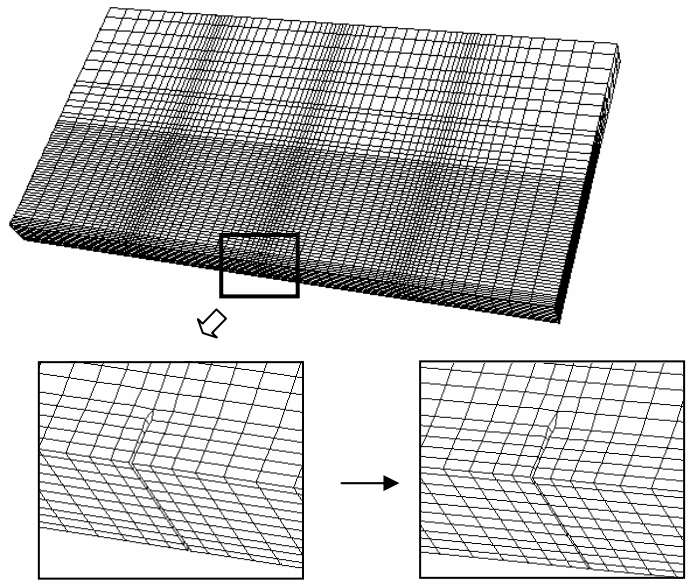

(a) Prior to crack propagation (b) after crack propagation

Figure 11 Modeling of crack growth of a through-thickness crack.

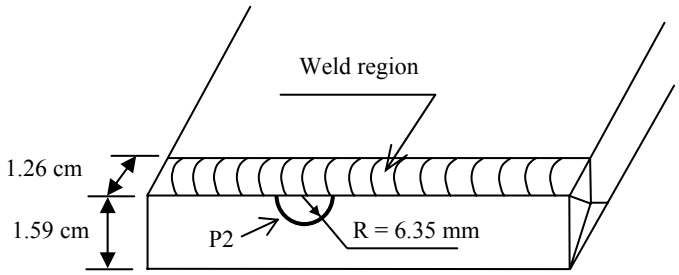


Figure 12 The cross-section view of a parallel crack (P2)

Effect of Seed Crack Fabrication Sequence. An attempt was made to investigate the cause of different final crack lengths for V1, V2, and V3, which are located in a relatively uniform residual stress field in an otherwise homogeneous material. A plausible scenario is the fabrication sequence of these seed cracks. The most logical sequences in a machine shop are:

Case 1: Fabrication Sequence - V2, V3, V1
Case 2: Fabrication Sequence - V3, V2, V1
Case 3: Fabrication Sequence - V1, V2, V3

The designation of the seed cracks is referenced with respect to the welding direction, as indicated in Figure 13 (also see Figs. 2 and 3).

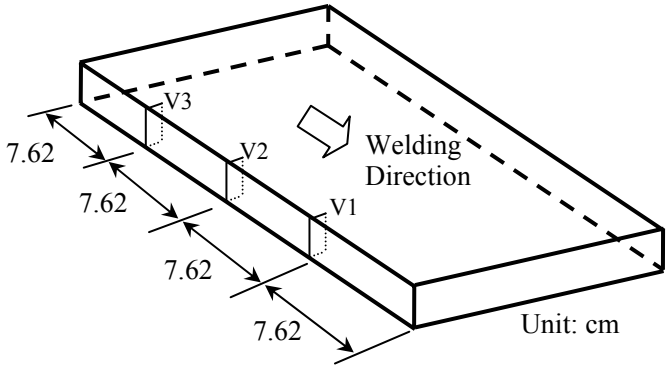


Figure 13 Designation of V1, V2 and V3 in the specimen plate.

Each case of the fabrication sequence of the cracks is modeled with the use of ABAQUS [1] solution mapping function. The initial stress for the calculation coincides with the as-welded residual stress. The stress intensity factors at the tips of the three cracks are calculated and plotted in Figures 14 to 16. Indeed the sequence to open the cracks in a plate affects the values of the stress intensity factors due to the inherent residual stress, which undergoes self-equilibrium. In particular, the highest K value always occurs in the last fabricated crack, which happened to be either V1 or V3, at either end of the test specimen. Judging from the cracking configuration in Figure 3, it seems that the seed cracks were fabricated by either Case 1 or 2. Unfortunately, the sensitivity of fabricating seed cracks was not expected prior to the testing. Therefore, the actual fabrication sequence is not retrievable.

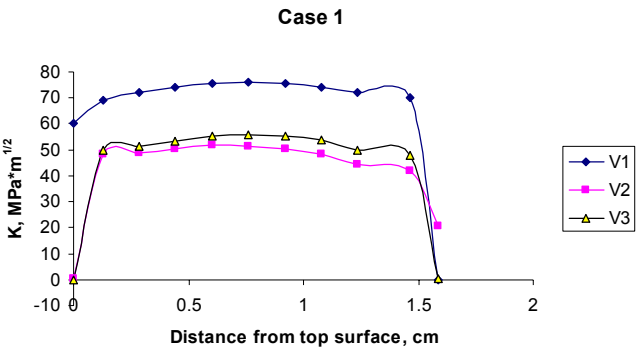


Figure 14 Seed crack fabrication sequence - V2, V3, V1.

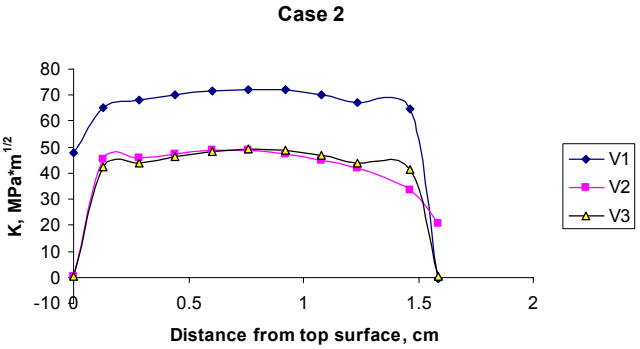


Figure 15 Seed crack fabrication sequence - V3, V2, V1.

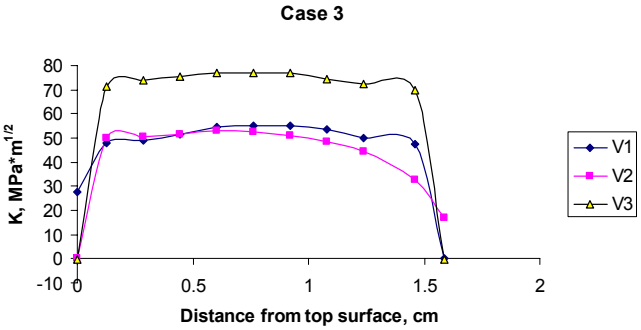


Figure 16 Seed crack fabrication sequence - V1, V2, V3.

Crack Propagation of a Vertical Crack (V2). From the analysis of the fabrication sequence, it was shown in Figures 14 to 16 that the stress intensity factor of the seed crack V2 is insensitive to the fabrication process. It is then chosen for a crack propagation analysis.

Following the same ABAQUS [1] procedure as described in previous sections, a through-thickness vertical crack across the weld is created in an initially intact plate with as-welded residual stress. The crack length is incrementally increased in a self similar manner (i.e., the crack front remains straight and through the thickness), resulting in a continuous redistribution of the residual stress. This allows the stress intensity factors at the crack tip nodes be calculated as a function of crack growth. The largest stress component is found to be the longitudinal stress ($\sigma_{xx}$) (see the Cartesian coordinate system identified in Figure 5). This stress component coincides with the Mode I opening stress for the crack V2. The other stress components are about 10% of $\sigma_{xx}$. Therefore, the crack extension is considered to be under Mode I, and the stress intensity factors calculated are in fact $K_I$.

Figure 17 shows the residual stress component ($\sigma_{xx}$) for Mode I crack extension of V2. The stress distributions due to crack growth (for crack lengths, respectively 1.2 and 6.8 cm) can be compared with that for the as-welded, crack-free plate (i.e., a= 0). The stress concentration near the crack tip is clearly shown.

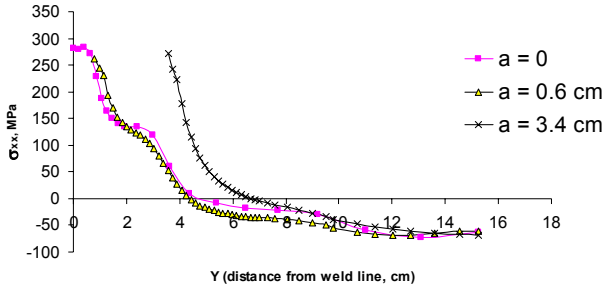


Figure 17 Distributions of the longitudinal residual stress $\sigma_{xx}$ for a non-cracked welded plate (a= 0) and for two crack lengths (1.2 and 6.8 cm)..

The calculated Mode I stress intensity factor as a function of crack extension is plotted in Figure 18. The K-value is calculated at the crack tip in the mid-thickness location of the finite element model. It appears that this residual stress field would drive the seed crack (V2) from the initial length of 1.27 cm (0.5 in.) to about 7.8 cm (3.1 in.) when the $K_{ISCC}$ is 35 MPa$\sqrt{m}$ (32 ksi$\sqrt{in}$) as determined previously from a test environment of 5M $NaNO_3$ solution at 100 °C [5]. In view of the amount of uncertain variables encountered during the testing, this crack length prediction agrees reasonably well with the test result, which indicates that the final crack length for V2 is about 5.9 cm (2.3 in.), as shown in Figure 3.

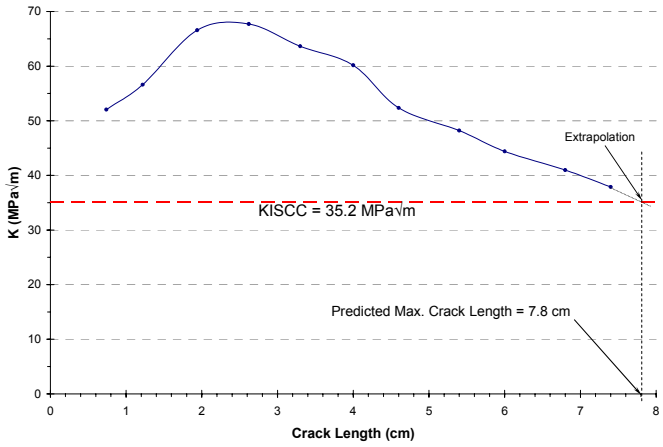


Figure 18 The calculated stress intensity factors (K) for V2 and final crack length prediction with $K_{ISCC}$.

## CONCLUDING REMARKS

The stress corrosion cracking specimens were prepared according to the specifications of the material (A285 Grade C carbon steel) and the welding procedure (GMAW) for the high level radioactive waste storage tanks built in 1950's. Various seed cracks were fabricated in the test plates to approximate the initial defects in the weld region of the storage tanks. The test specimens were exposed to an aggressive chemistry solution that is known to promote nitrate stress corrosion cracking. The experiment showed that the stress corrosion cracking indeed occurred in the non-stress relieved, as-welded test specimen. The crack lengths were measured and confirmed by UT and MT, and are compared with the theoretical prediction from a series of three-dimensional finite element analyses which include welding simulation, residual stress determination, and crack propagation analysis. The predicted crack length is based on a $K_{ISCC}$ determined in an earlier test under similar exposure condition for A285 carbon steel. The agreement between the predicted and the measured crack lengths is considered satisfactory, considering the nature of uncertainty encountered during the material selection, specimen preparation, testing condition, actual cracking configuration, and the welding parameters of the GMAW process. The experimental investigation has substantiated the effectiveness of stress relief, and provided insight to the stress corrosion cracking in carbon steel under a corrosive environment. The numerical procedure is adequate to model the welding and the crack propagation. The numerical simulation of seed crack fabrication has demonstrated that the details of specimen preparation might affect the interpretation of test data. The accuracy of prediction can be improved by a careful design of experiment and specimens. A

complete documentation of welding and specimen fabrication may be important in resolving the discrepancies between the test data and prediction. A finite element model with mesh refinement, especially in the cracking region and near the specimen free surfaces, will further improve the accuracy of prediction.

## ACKNOWLEDGMENTS

PSL, RLS, TMS, and JBE of the Savannah River National Laboratory (SRNL) acknowledge the support from the United States Department of Energy (DOE) Office of Science Environmental Management Science Program (EMSP), and from DOE under Contract No. DE-AC09-96SR18500 to the Westinghouse Savannah River Company. CC and YJC of the University of South Carolina were supported by the U. S. National Science Foundation grant CMS0116238.

## REFERENCES

[1] ABAQUS Standard Version 6.2-1, 2001, ABAQUS Inc., Pawtucket, Rhode Island.

[2] Chao, Y.J., Zhu, X.K., Qi, X., 2000, "WeldSim—A WELDing SIMulation Code for the Determination of Transient and Residual Temperature, Stress, and Distortion," Advances in computational Engineering and Science, Vol II, Editor: Atluri, S.N. and Brust, F.W., pp. 1206-1211.

[3] Chao, Y.J., Qi, X., 1999, "Three-dimensional Modeling of Gas Metal Arc Welding Process," NAMRC XXVII, Berkeley, California.

[4] Chao, Y.J., Qi, X., Tang, W., 2003, "Heat Transfer in Friction Stir Welding - Experimental and Numerical Studies," Transaction of ASME, Journal of Manufacturing Science and Engineering, Vol 125, pp. 138-145.

[5] Zapp, P. E. and Lam, P.-S., 2000, "Preliminary Evaluation of Tank 15 Vapor Space Cracking," WSRC-TR-2000-00187, Westinghouse Savannah River Company, Aiken, SC 29808.

[6] Donovan, J. A., 1977, "Materials Aspects of SRP Waste Storage – Corrosion and mechanical Failure," DP-1476, E. I. du Pont de Nemours and Company, Savannah River Laboratory, Aiken, SC 29801.

[7] Cheng, C., 2004, "Finite Element Modeling of Gas Metal Arc Welding and Stress Corrosion Cracking in Welded Plate," MS Thesis, University of South Carolina, Columbia, SC 29208.

[8] Mohammad, S. D., 1999, "A Comprehensive Study of Gas Metal Arc Welding Process: Finite Element Simulations and Experiments," Ph.D. Dissertation, University of South Carolina, Columbia, SC 29208.

[9] Incropera, F. P. and DeWitt, D. P., 1996, FUNDAMENTALS OF HEAT AND MASS TRANSFER, 4th edition, John Wiley & Sons, New York, NY.

[10] Dike, J., Cadden, C., and Corderman, R., 1995, "Finite Element Modeling of Multipass GMA Welds in Steel Plates," Trends in Welding Research, Proc. Of the 4th Inter. Conf., Gatlinburg, Tennessee.

[11] Fanous, I. F., Younan, M. Y., and Wifi, A. S., 2003, "Study of the Effect of Boundary Conditions on Residual Stresses in Welding Using Element Birth and Element Movement Techniques," Journal of Pressure Vessel Technology, Transaction of ASME, Vol 125, pp. 432-439.

[12] Fanous, I. F., Younan, M. Y., and Wifi, A. S., 2003, "Three Dimensional Finite Element Modeling Of The Welding Process Using Element Birth And Element Movement Technique," Journal of Pressure Vessel Technology, Transaction of ASME, Vol 125, pp. 144-150.

[13] Dong, P. and Rawls, G. B., 2003, "Crack Growth Behavior in a Residual Stress Field for Vessel Type Structures," ASME Pressure vessel and pipes conference, Vol 464, Residual Stress, Fitness-for-Service, and Manufacturing Processes, pp. 43-57.